Applied Catalysis A, General 592 (2020) 117440

Contents lists available at ScienceDirect

Applied Catalysis A, General

journal homepage: www.elsevier.com/locate/apcata

Selective transformation of ethanol to acetaldehyde catalyzed by Au/h-BN interface prepared on Rh(111) surface

Arnold P. Farkas[a,b,*], Ádám Szitás[c], Dániel Jurdi[d], Krisztián Palotás[a,e], János Kiss[a], Zoltán Kónya[a,c]

[a] MTA-SZTE Reaction Kinetics andSurface Chemistry Research Group, University of Szeged, Rerrich Béla Square 1, Szeged, 6720, Hungary
[b] Extreme Light Infrastructure – Attosecond Light Pulse Source, ELI-HU Non-Profit Ltd., Dugonics Square 13, Szeged, 6720, Hungary
[c] Department of Applied and Environmental Chemistry, University of Szeged, Rerrich Béla Square 1, Szeged, 6720, Hungary
[d] Department of Physical Chemistry and Materials Science, University of Szeged, Rerrich Béla Square 1, Szeged, 6720, Hungary
[e] Institute for Solid State Physics and Optics, Wigner Research Center for Physics, P.O. Box 49, Budapest, 1525, Hungary

ARTICLE INFO

Keywords:
Ethanol
Rh(111)
Au nanoclusters
Boron nitride
HREELS
DFT

ABSTRACT

Controlled shape and size distribution of metal nanoparticles for surface catalytic reactions are important. Through deposition onto the periodic surface of h-BN we can adjust these parameters of gold thereby we are able to influence the catalytic activity of the nanoparticles. In this study we investigated the decomposition of ethanol on gold nanoparticles supported on h-BN/Rh(111). High-resolution electron energy loss spectroscopy (HREELS) and temperature programmed desorption (TPD) methods have been used on the experimental side. Ethanol showed enhanced stability on Au/h-BN/Rh(111) system. The stabilization effect increases with gold coverage and saturates before gold reaches a continuous adlayer. High selectivity was observed towards "CO free" hydrogen, a small part of ethanol dissociated to hydrogen and acetaldehyde without further decomposition. Density functional theory (DFT) calculations delivered important information about the adsorption characteristics of ethanol and hydrogen on model Au/h-BN/Rh(111). The importance of low-coordinated negatively charged Au atoms is confirmed by DFT results.

1. Introduction

There are several interesting layered systems, such as two-dimensional (2D) graphene-like honeycomb structure made up of materials other than carbon. They have novel properties associated with these 2D systems and they can raise a lot of potential application possibility in nanotechnology. Hexagonal boron nitride (h-BN) is applied in many technological processes in recent years, owing to its interesting electronic and chemical properties. The h-BN structure is composed of alternating nitrogen and boron atoms [1–4]. Its electronic properties are very different from the semi-metal graphene, that is, h-BN is an insulator with a band gap of ~6 eV; this value shows slight variation with dimensionality [4–7]. One promising application is its use as a dielectric material for future graphene-based transistors, recently it was shown that graphene can be grown on h-BN directly [8–11]. BN monolayers (MLs) are promising insulator components for nanoelectronics. When prepared on certain low index transition metal surfaces, like Rh(111), a periodic buckling of the single h-BN layer takes place, and a so-called nanomesh is formed consisting of "wires" and "pores" [12,13]. This feature allows its application as a nanotemplate with a hexagonal periodicity of 3.2 nm [14], with implications for plasmonics as well. Furthermore h-BN is also a useful support in heterogeneous catalysis as a well-known chemically inert material which does not interact electronically with the supported molecules or metal nanoparticles [15]. BN can substitute the oxide support in heterogeneous catalysis neglecting the undesirable oxide-metal interactions.

It turned out that gold nanoparticles exhibit unusually high activity in many reactions studied recently. Au performed an outstanding catalytic effect for catalytic reactions, oxidation of different hydrocarbons, hydrogenation of unsaturated hydrocarbons and elimination of NO_x [16]. Au clusters in small sizes effectively catalyze the reaction between carbon monoxide and oxygen even at low temperatures [17]. The Au cluster sizes showed significant differences in the reaction rate in CO oxidation, maximum reaction rate was reached at ~3.5 nm cluster size [18]. There are different interpretations in the literature for this effect. Some researchers emphasize the role of sites at the metal/support

* Corresponding author at: MTA-SZTE Reaction Kinetics and Surface Chemistry Research Group, University of Szeged, Rerrich Béla Square 1, Szeged, 6720, Hungary.
E-mail addresses: arnold.farkas@chem.u-szeged.hu, arnold.farkas@eli-alps.hu (A.P. Farkas).

https://doi.org/10.1016/j.apcata.2020.117440
Received 26 November 2019; Received in revised form 21 January 2020; Accepted 22 January 2020
Available online 23 January 2020

interface [19] and others suggested the importance of coordinative unsaturation of the surface atoms [20]. Goodman and coworkers ascribed the anomalous high activity of small clusters to quantum-size effects based on their Scanning Tunneling Microscopy (STM) results [21]. Recently it was presented that small Au clusters supported on titania–like oxide (titanate nanotubes) play an important role in photocatalytic transformation of CH_4 and CO_2 [22–24]. It was suggested that molecular-like gold clusters in the Au_{25} form are directly involved in the photo-assisted reaction, namely in the activation of the CH_4/$Au_{25}\delta^+$ surface complex with light irradiation. There is also an interesting result that sub-nanosized gold on titanate nanotubes performs an outstanding activity in CO_2 hydrogenation. The important finding is that fundamental differences were observed in the thermal activation and photocatalytic process [24]. In thermal reaction, exclusively CO and water were the products, while in photo-induced reaction the methane formation was the dominant route. Recently scanning probe techniques (STM) gave a useful information about the surface properties of supported Au nanoparticles as a function of the number of Au atoms [25,26]. It was pointed out that the shape of nanoparticles of the admetal determines the charge transfer from the support to the metal particle and from the metal to the oxide support. The chemical potential as a function of particle size of gold was reported from the single atom to the bulk like limits [27]. Recently, the metal-containing heterogeneous catalysis was surveyed from single atoms to nanoclusters and nanoparticles [28]. Metallic species of different size exhibited basic differences in heterogeneous catalytic reactions.

Surprisingly, there are just a few papers dealing with the reaction of alcohols including ethanol, C_2H_5OH, on gold catalysts. The study of the catalytic transformations of ethanol, partial oxidation, steam and dry reforming, are very important issues because they can be the source of hydrogen production for the alternative energy [29–31]. On the other hand, ethanol can serve as an important starting material for different chemicals such as aldehydes, ketones and others. In these procedures the C—C and C—O bond breaking, C—C bond preservation and successive dehydrogenation of ethanol have importance with different emphasis and purpose. On noble metals supported on reducible oxides the C—C bond rupture and dehydrogenation occur producing hydrogen as potential fuel [32–34]. Using acidic support the preferential product is the ethylene [35–37]. On basic properties support, like CeO_2, oxidation, coupling and ketonization may occur and acetone and other oxygen containing compounds are the products of ethanol reformation [38–40]. On metals supported on silica-like support the acetaldehyde is the main end product in ethanol decomposition but CO, CO_2 and C_xH_y are also formed [34,39,41]. From these observations the main conclusion is that the support may influence the ethanol transformation reactions.

Earlier, Idriss et al. [42] investigated the oxidation of ethanol on Au/CeO_2, and later Guan and Hensen [41] studied the dehydrogenation of C_2H_5OH on Au nanoparticles deposited on various SiO_2 supports. A strong effect of the Au nanoparticle size was observed. Solymosi et al. [39] studied the adsorption and decomposition of ethanol on Au supported different oxides. They found that the product distribution strongly depends on the nature of the support. In order to establish the role of gold nanoparticles it is worth to study the interaction of ethanol using a practically inert support. For this purpose the boron nitride (BN) would be a good candidate [15]. The choice of boron nitride is promising but there is not a hundred percent guarantee for the full inactivity in certain cases as it was presented recently that the boron nitride is an excellent catalyst for selective oxidative dehydrogenation of propane to propene [43,44]. Beside this very important catalytic behaviour of BN, it was concluded that C—C bond rupture – which is an important step in ethanol decomposition - was not detected in the present study.

Now, the metal-support interaction can be minimized on two non-oxide supports (graphene and BN). Graphene is in the focus of research and it is suitable to control the growth of metal particles including Au [45–47]. From this respect, the other important support is the BN prepared on single crystal surfaces. The h-BN nanomesh template provides the possibility to produce Au nanoparticles in quasi uniform size and ordering determined by the pore of BN. The h-BN/Rh(111) system is very interesting since Corso et al. [12] discovered a self-organized boron nitride superstructure on a Rh(111) surface. It exhibits a h-BN nanomesh, a highly corrugated superstructure, into which the metal nanoparticles including Au can be readily adsorbed and thus arranged at the atomic length scale [48–51]. The previous density functional theory (DFT) calculations and experimental results indicated an excess negative charge on small Au nanoparticles on the h-BN/Rh(111) nanomesh [50,51].

In this study we investigate the activation and decomposition of ethanol on Au/h-BN interface formed on Rh(111). We collected information about ethanol-gold interaction without any disturbing effect of an oxide support. Auger electron spectroscopy, high-resolution electron energy loss spectroscopy and temperature programmed desorption methods have been used. Very recently acetaldehyde – a transient or final product of ethanol transformation – was investigated on Au/h-BN/Rh(111) with the same methods [52]. The acetaldehyde can be activated on gold nanoparticles especially on the edge and corner atoms. However, C—C cleavages were not observed.

2. Experimental and computational details

The UHV system -which we used in these studies- and its operation was described previously [52]. In the reaction chamber the base pressure of 5×10^{-10} mbar was ensured by a turbomolecular pump and a set of surface analytical technics were installed, like AES, HREELS and Temperature Programmed Desorption (TPD). The HREEL spectrometer (LK, ELS 3000) has a routine resolution of $20-40\,cm^{-1}$ (FWHM). The elastic peak intensity was in the range of 1×10^4–1×10^5 counts per second (cps), nevertheless we normalized the elastic peak intensities to the same value, thereby creating comparability. Spectra were recorded in the specular direction (angle of incident was 60° to the surface normal) with a primary beam of 6.5 eV. A Balzers quadrupole mass spectrometer was used for TPD measurements. The heating rate was 4 K/s.

The Rh(111) single crystal was a product of Materials Research Corporation (purity 99,99 %). Before all experiment series the sample was cleaned by Ar^+ sputtering (typically 1 kV, 1×10^{-7} mbar and 2 μA for 10 − 30 min) and annealing cycles at 900 − 1100 K until no contaminations were detected by Auger spectroscopy. The sample temperature was variable between 140 and 1200 K wich we reached by resistive heating. Ethanol (CH_3CH_2OH) of 99 % purity was the product of Sigma Aldrich and it was dosed through a capillary.

Au deposition was made by a physical vapor deposition (PVD) source (Oxford Applied Research) using high-purity (99.95 %) Au. The coverage of gold is given in monolayer equivalent (MLE), defined as the surface concentration of Rh(111): $1.60 \times 10^{15}\,cm^{-2}$ [53]. During experiments the evaporation rate was ~0.2 MLE/min. Preparation temperature of the h-BN monolayer was at 1000 − 1050 K via thermal decomposition of > 99.8 % purity borazine, a product of Katchem Ltd.

In order to gain a theoretical insight into some of the experimentally obtained results, extensive DFT calculations were performed. The Vienna Ab initio Simulation Package (VASP) [54,55] was used with the projector augmented wave (PAW) method [56] to describe the electron-ion interaction, and with the optB86b-vdW functional [57,58] to account for dispersion correction.

A supercell slab is modelled as three Rh atomic layers in (111) crystallographic orientation, consisting of 12 × 12 Rh atoms each (with the experimental lattice constant of Rh: 2.689 Å), followed by the h-BN overlayer in a 13 × 13 superstructure, corresponding to the lattice mismatch of Rh(111) and h-BN [13]. This way, 770 (3 × 144 (Rh) + 2 × 169 (B + N)) atoms were included in the supercell [51]. This h-BN/Rh(111) structure was used as a starting point for further modelling

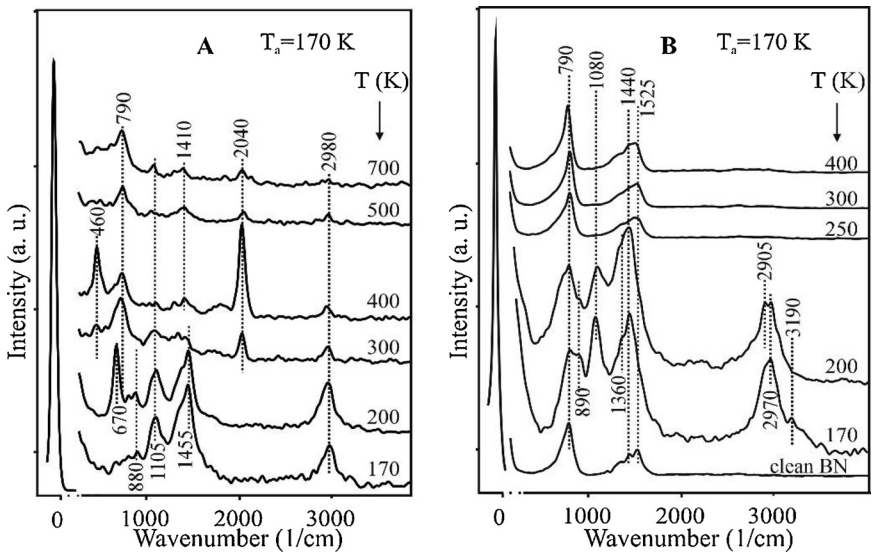

Fig. 1. Effect of annealing on the HREEL spectra after adsorption of 4 L ethanol at 170 K on the clean (A) and h-BN monolayer covered Rh(111) surface (B).

of several systems, which are relevant for the presented experimental analysis:

(1) Au_1/h-BN/Rh(111): Au adatom adsorption on the h-BN/Rh(111) to find the favoured starting point for Au atomic cluster (or nanoparticle) growth. Nine adsorption positions were considered, from those six on-top positions: pore-N, pore-B, wall-N, wall-B, wire-N, wire-B, and three hollow positions above the middle of BN hexagonal rings: pore-h, wall-h, wire-h. Note that "wall" is in between "pore" and "wire" regions.
(2) Au_{19}/h-BN/Rh(111): Adsorption of a Au island consisting of 19 atoms to model differently coordinated Au atoms in the pore of the h-BN/Rh(111). This Au_{19} island is centred above the energetically favoured Au_1 position on h-BN/Rh(111) based on the results obtained in point (1). The Au_{19} island is initially modelled as a flat atomic island consisting of 1 (Au-m: middle at favoured Au_1 position) + 6 (first shell) + 12 (second shell) Au atoms. From the second shell six atoms are edge atoms (Au-e) with two Au neighbours in a line within the same shell, and six atoms are vertex atoms (Au-v) with two Au neighbours not in line within the same shell.
(3) H/h-BN/Rh(111): Hydrogen adatom (reaction product) adsorption on the h-BN/Rh(111). Nine adsorption positions were considered, the same as in point (1).
(4) H/Au_{19}/h-BN/Rh(111): Hydrogen adatom adsorption on the Au_{19}/h-BN/Rh(111). Nine adsorption positions were considered, from those six above the h-BN nanomesh: wall-N, wall-B, wall-h, wire-N, wire-B, wire-h (see point (1) for explanation), and three above the Au_{19} island: Au-m, Au-e, Au-v (see point (2) for explanation).
(5) Ethanol/h-BN/Rh(111): Five differently oriented ethanol molecules were adsorbed above six characteristic on-top positions of the h-BN nanomesh: pore-N, pore-B, wall-N, wall-B, wire-N, wire-B (see point (1) for explanation). Altogether 30 adsorption configurations were considered.
(6) Ethanol/Au_{19}/h-BN/Rh(111): Five differently oriented ethanol molecules were adsorbed above seven surface sites, from those four characteristic on-top positions of the h-BN nanomesh: wall-N, wall-B, wire-N, wire-B (see point (1) for explanation), and three above the Au_{19} island: Au-m, Au-e, Au-v (see point (2) for explanation). Altogether 35 adsorption configurations were considered.

In all of the above considered systems (1)-(6) a vacuum layer of at least 16 Å thickness was included in the perpendicular (111) direction to avoid interactions between periodic supercell slabs. The bottom Rh layer was fixed and all other atoms were let to be freely relaxed during the geometry optimizations, where the force convergence criterion acting on individual atoms was 0.02 eV/Å. The Brillouin zone was sampled by the Γ point only due to the large size of the supercell. When calculating the adsorption energies, Bader charges, [59–61] and charge transfer, a k-point sampling of 3 × 3 × 1 has been applied. Reported total energy differences correspond to the whole supercell.

3. Results and discussion

3.1. Adsorption of ethanol on clean Rh(111) and the effect of BN monolayer on the reactivity of the single crystal

Ethanol chemistry on Rh single crystal surfaces was investigated previously in a plenty of excellent works [62–64]. Nevertheless the outlined two way dissociation mechanism in the study of Houtman and coworkers [64] spurred our intention to follow the adsorption and reactions of ethanol on clean Rh(111) surface, too. Similarly to the literature data we observed C—C bond breaking, CO and H_2 desorption after adsorption of ethanol on a clean Rh(111) surface. Furthermore, the desorption of CH_4 was also detected in smaller quantity, which is produced probably through η^2-acetaldehyde formation. The open question was whether the reaction route which led to these products contains the $CH_2CH_2O_a$ surface intermediate form or not. Observation of the proposed intermediate –oxometallacycle- in HREELS is not easy because after its formation it decomposes further immediately. Increasing the temperature of the adsorbed molecular layer above 200 K (see Fig. 1A) we observed several characteristic vibrations which very likely belong to η^2-(O,C) – CH_3CHO at 670, 1105, 1195, 1340, 1410, 2890 and 2980 cm^{-1} in harmony with our former work after acetaldehyde adsorption on clean and modified Rh(111) surfaces [65], see Table 1. Another remarkable finding at room temperature (RT), similarly to Pt(111) single crystal surfaces [66], is that the clean rhodium surface acts as a good C—C breaking catalyst. We can recognize the clear sign of this as the adsorbed CO appears at 2040 cm^{-1}. Nevertheless, HREEL spectra at this latter temperature is very complex suggesting the presence of different type of surface intermediates, too. In the work of Barteau the spectral sign of oxometallacycle was discovered at 450, 860, 1090, 1475, 2850 – 2950 cm^{-1} [66,67]. If we investigate the spectra (Fig. 1A) in detail, we can observe peaks at these wave numbers but we cannot distinguish them without doubt from the other peaks.

If we cover the clean rhodium surface with one monolayer of h-BN

Table 1
Characteristic vibrations of ethanol and its reaction intermediates.

Vibrational modes	CH_3CH_2OH on Rh(111) [64]	CH_3CH_2O(a) on Rh(111) [64]	$-OC^1H_2C^2H_2-$ on Ag(110) [69]	η^2(C,O)-CH_3CHO on Rh (111) [64]	*This study* 4 L of Ethanol on BN/Rh(111) below 250 K
ν (OH)	3270				3190
ν_a (CH_3)	2990	2990			2970
ν_a (C^1-H)			2922		
ν_s(C^2-H)			2922	2980	
out of phase χ (CH_2)			1446		
ν(CO)				1460	
in phase χ (CH_2)			1446		
δ (CH_2)	1490	1405			1440
δ_s (CH_3)	1380	1390		1380	1360
w(C^1H_2), tw (C^2H_2)			1353		
w(CH_2)			1273		
tw (C^1H_2)			1218		
ν (CO),ν_a (CCO)	1070	1070			1080
ν_a (O-C^1-C^2)			1052		
ν_a (O-C^1-C^2)			996		
ν (CC), ν_s (CCO), ρ (CH_3)	890	880		1135 950	890
γ (OH)	815				
ν_s (O-C^1-C^2)			793		
δ (CCO)	480	510		610	
ν_s (Ag-O), (Ag-C^2)			344		

before adsorbing ethanol, dramatic changes occur (Fig. 1B). The preparation method and characterisation of a 2D BN layer on Rh(111) was reported in our former studies in detail [65,68] but as a brief introduction we can summarize here that on the HREEL spectra of h-BN the peak at 790 cm^{-1} corresponds to a transverse optical (TO) phonon with an out-of-plane polarization. The features at 1350 and 1510 cm^{-1} are assigned to phonons with an in-plane polarization; the former one is originated from the transverse optical phonon, while the other one from the longitudinal optical (LO) phonon. Adsorption of ethanol on this 2D monolayer at 170 K and subsequent heating of the layer showed that the interaction of ethanol with BN is very weak. The losses belong to molecularly adsorbed ethanol appeared (see Table 1), however ethanol desorbed intact completely below 250 K from the surface. These results suggest not only the inertness of the BN layer toward ethanol dissociation but also the lack of substrate metal effect through boron nitride layer toward the chemisorption of ethanol.

3.2. Stability of ethanol on gold decorated h-BN/Rh(111) surfaces

On the clean Rh(111) surface, the ethanol multilayer (above exposure of 1.1 L) starts to desorb at around 150 K. However, ~58 % of the chemisorbed monolayer desorbed molecularly at T_p = 210 K with a peak which has a very long tail even up to 500 K. The remaining part of the ethanol underwent dissociation. Our results from the clean surface agree well with the above shortly introduced TPD data [64]. In the light of the observed inert behaviour of a clean BN monolayer on Rh(111) we turned to the study of the gold-decorated BN/Rh(111) surfaces and the adsorption properties of ethanol on them. We registered the ethanol stability at increasing gold coverages on the BN nanomesh first by TPD method (Fig. 2A). Investigating the changes at the atomic mass unit corresponding to ethanol we observed a downward (~25 K) shift in the low temperature (250 K) peak temperature maximum on the boron nitride compared to the clean Rh(111) layer. The lowered stability on the BN surface is not a surprise taking into account the above-mentioned weak interaction between the substrate and the molecules at this temperature. Our calculation results (detailed information in Section 3.4) also showed a weak and an energetically uniform interaction between ethanol and BN nanomesh adsorption regions. These results are in contrast with our observations concerning another organic molecule (azobenzene) adsorption on the same nanomesh surface. In that case we were able to distinguish energetically diverse adsorption regions on the BN nanomesh (wire, wall and pore sites).

When we evaporated gold onto the BN surface the desorption temperatures shifted back to the value observed on the clean Rh(111) and a shoulder appeared at Tp = 280 K at one monolayer gold coverage. Although the peak maxima are around 250 − 280 K the TPD results represent a wide desorption range with an elongated tail on the peak curve at higher temperatures. These results are in very good harmony with our HREEL spectroscopic observations (Fig. 2B and C). In Fig. 2B we exhibit HREEL spectroscopic data as a function of gold coverage at 250 K surface temperature. At this temperature the multilayer ethanol has already desorbed so we can easily compare the amount and state of chemisorbed molecules remaining on the surface.

Although the features at around 800 and 1400 − 1500 cm^{-1} (h-BN phonon modes) are very strong and dominated the spectra we can also discover peaks at around 1030 and 2950 cm^{-1} related to ν(CCO) and ν(C–H) vibrations of ethanol molecules or ethoxy on the gold covered BN surfaces. As discussed in section 3.1. we did not observe ethanol adsorption above 200 K on the clean h-BN layer. When we increase the gold coverage the contribution of ethanol related peaks at 250 K becomes stronger along the BN phonon vibrations. Moreover above 4.5 MLE the phonon peaks lost their dominance and the ethanol-related features dominate the spectra. The reason is very likely that the gold layer covered the BN nanomesh completely. Nevertheless, the latter gold layer and its adsorption behaviour differ from the gold single crystal. Namely, our measurement on Au(111) surface (Fig. 2B) shows the complete disappearance of ethanol contributions at this temperature. On Au(111) even at 180 K almost all of the ethanol desorbed intact from the unmodified single crystal. Fig. 2C shows the peak intensity values of the observed ethanol vibration peaks as a function of gold coverage. We can identify a growing trend, with the increasing number of gold clusters (the growth of gold clusters was investigated by STM in detail in our previous paper [51]) the normalized peak intensities are also increased. Nevertheless, the lack of defect or specific/low coordinated gold adsorption sites causes a significant drop in ethanol stability on Au(111) single crystal. We step-wisely added several monolayers of gold onto the BN layer, this way we gradually filled up not only the pores but covered also the wire regions. We expected a specific gold coverage where we reach a maximum in the amount of adsorbed ethanol. In other words, we looked for a specific gold coverage but at 250 K there were no signs of prominent ethanol stability. However, we can observe a plateau between 0.2 and 1.0 MLE of Au,

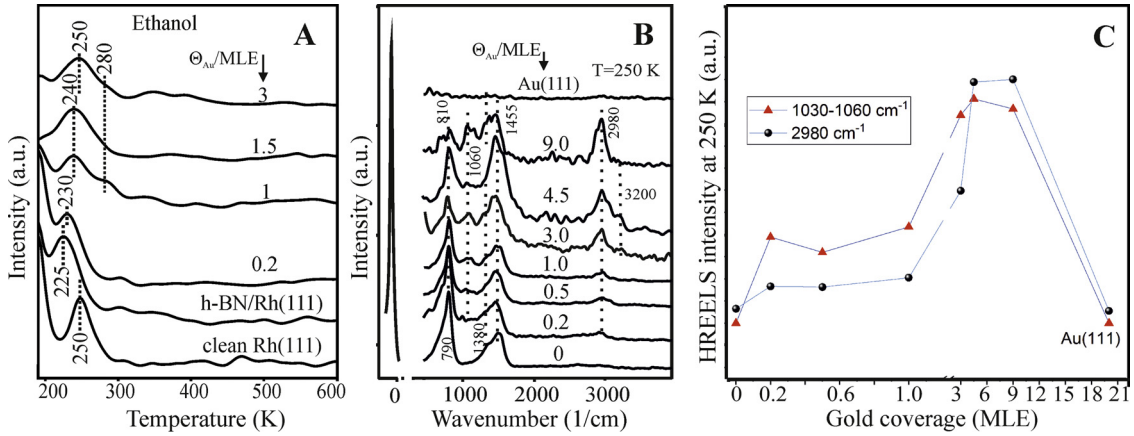

Fig. 2. Effect of gold coverage on the desorption of ethanol (amu 31) after adsorption of 4 L ethanol at 170 K on the clean and gold covered h-BN/Rh(111) (A). HREEL spectra (B) and changes in the intensity of HREELS peaks (C) of the ethanol/h-BN/Rh(111) adsorption layer at 250 K at different gold coverages.

where the peak intensities are approximately unchanged. On the h-BN nanomesh surface the growth of Au at room temperature leads to the formation of mainly three-dimensional (3D) gold nanoparticles, although at low coverages (0.2 MLE) 2D particles formed as well and starts first in the pore regions [51,52]. Our calculations also confirm this, namely the on-top boron positions in the pores are the energetically favoured positions for gold clusters (detailed information in Section 3.4). The oriented, in fact a forced Volmer-Weber, growth mode in the pores limits the number of available gold adsorption sites while its coverage is still increasing. Furthermore, at 250 K only the stabilized ethanol molecules can exists on the surface which need specific low coordinated metal atoms very likely positioned at the perimeter of the gold clusters or at the interface of gold and BN (in good agreement with our calculation results see below at Fig. 6B). This can be a possible explanation why the peak intensities connected to the adsorbed ethanol on the 250 K surface do not increase below 1 MLE of gold. At 1.0 MLE the size distribution, not only the height but the diameter of the Au nanoparticles is fairly wide, the highest particles are made up of 4–5 layers and their diameter is around 4–5 nm [51]. When increasing the coverage to 3.2 ML this trend continues, where the largest particles consist of 8–9 atomic layers, their diameter is around 6–7 nm and the particle density is around 1.8×10^{12} cm^{-2}. Nevertheless, when the coverage is higher (above 1.0 MLE) the amount of stable ethanol increases further until we reach saturation at around 6 MLE. Above this gold coverage the number of adsorption centres at the BN-gold interface are constant because of the 3D growth mode. The need for low coordinated gold atoms is verified by our experiments on the Au(111) surface where the adsorption probability for gold above 200 K dropped back to the value of clean h-BN.

3.3. Effects of gold on the reaction route of ethanol on BN/Rh(111)

In the light of the results connected to the enhanced ethanol stability on the gold-modified surface it was expected that we can count with surface reactions and not just by the complete molecular desorption as it was observed on the clean BN surface. On rhodium and on other noble metal surfaces C—C bond rupture takes place above 200 K [64–66]. To follow the reactions on the investigated layer we collected TPD data at different gold coverages and we looked for all the possible reaction products (ethanol, CO, H_2, acetaldehyde, CH_4, H_2O). Among molecular ethanol desorption – practically finished below 300 K- we detected hydrogen and acetaldehyde desorption at amu 2 and 29 simultaneously at around 300 and 400 K from the 1.5 MLE gold covered nanomesh surface (see Fig. 3A). This suggests a dehydrogenation reaction supported by gold nanoparticles. In the literature of gold nanoclusters, it is not a surprise that gold acts as a catalyst which supports that reaction route. A. Gazsi and coworkers in their study compared the catalytic activity of gold nanoparticles on several supports [39]. They concluded that on almost all types of support gold clusters are active in the dehydrogenation process and as a first step adsorbed ethoxy is produced while at and above 400 K acetaldehyde (sometimes only as an intermediate) and hydrogen are generated. Another interesting feature in our measurements following the coverage dependency is that a measurable amount of acetaldehyde was detected only at a certain coverage range (Fig. 3B). We detected acetaldehyde in our measurements only at and below 1.5 MLE, and above these coverages we did not observe it, or it was under the detection limit of our technique. Based on our previous STM results at this coverage range (around 1–1.5 MLE) gold clusters have already filled almost all of the pores on h-BN, the size (4 − 5 nm) and decoration of the nanoparticles are in harmony with the nanomesh structure. A possible explanation for this coverage-dependent reaction is that the active sites of gold clusters on h-BN are very likely the edge and corner atoms on the interface of gold/BN nanomesh at small coverages. We also need to count with a charge transfer between the substrate and gold which also takes place at lower coverages and resulted in negatively charged particles. The negative charging of Au clusters was also strengthened by our high resolution electron energy loss spectroscopy (HREELS) measurements, because the stretching vibration of adsorbed CO on Au/h-BN/Rh(111) was found at a lower wave numbers (2090 cm^{-1}) at 0.2 MLE, while it was observed at 2125 cm^{-1} at 1 MLE (not shown). XPS measurements of the deposition of Au on the nanomesh at room temperature revealed a rather low Au 4f7/2 binding energy (83.55 eV) at 0.045 MLE as well. At higher gold coverage, as expected, the Au 4f7/2 peak gradually approached the bulk value [51].

In order to identify surface intermediates in the dehydrogenation process we analysed the HREELS results during annealing the 1 MLE and 4.5 MLE gold promoted layer with 4 L of ethanol (Fig. 4A and B).

In both cases, after ethanol adsorption we can observe the absence of ν(OH) vibration at 3300 cm^{-1} above 250 K and the characteristic vibrations of ethoxy dominated the spectra. While at one monolayer gold these spectral features are observed even until 500 K, at higher coverage they are hardly detectable above 300 K. This diversity at different coverages also shows the size effect of gold in the investigated process as we discussed above concerning the surface stability of ethanol. In connection with the evanescence of the OH vibration, another small but clear loss appears at 1 MLE at and above 250 K near ~2660 cm^{-1}. The latter peak belongs to the vibration of B–H bond. This suggests that the eliminated hydrogen from the ethanol migrates to the neighbouring boron atoms. Our DFT results also strengthen the possibility and the existence of the driving force toward this namely the hydrogen atom on the gold covered BN/Rh(111) likes to be located on

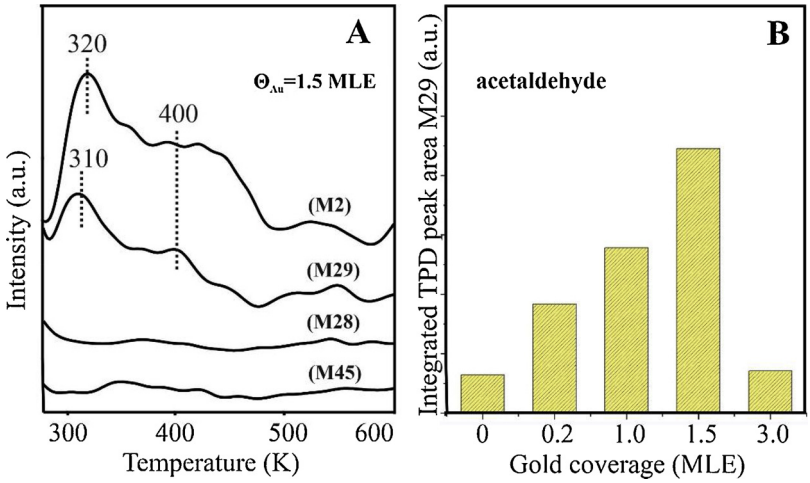

Fig. 3. Desorption spectra after adsorption of 4 L ethanol at 170 K on the 1.5 MLE gold covered h-BN/Rh(111) (A) and the changes in the TPD area of amu29 peak at different gold coverages (B).

boron or we can also say that the lowest energy option for the hydrogen at this surface is on a boron atom which is a neighbour of a gold cluster.

Another obvious remark is that on gold-covered BN/Rh(111) the reaction stops at the first dehydrogenation step, if we consider that we did not observe any sign of CO_a on HREEL spectra on BN containing surfaces. In other cases – e.g. on clean Rh(111)- when the C—C bond breaking is advantageous it was clearly observed at 2040 cm^{-1} (Fig. 1A). It also suggests that carbon-carbon bond cleavage did not happen on clean or on gold modified h-BN. Absence of CO_a is quite obvious as it is not stable neither on gold nor on BN at this temperature [70]. Beyond that we did not observe any other sign of surface intermediates (C–H fragments) resulting from the carbon-carbon bond rupture. While TPD clearly showed the production of acetaldehyde we cannot say that we were able to resolve the acetaldehyde losses in the annealing spectra. The losses of adsorbed acetaldehyde are very close to ethanol/ethoxy and we need to take into consideration the BN phonon losses which complicated the picture. Uncertainty in the identification of the acetaldehyde intermediates on the HREEL spectra could also be the consequence of the immediate desorption of acetaldehyde after surface production. In order to describe the formation of the above product we may assume the occurrence of the following elementary surface reactions:

$$C_2H_5OH_{(g)} = C_2H_5OH_{(a)} \quad (1)$$

$$C_2H_5OH_{(a)} = C_2H_5O_{(a)} + H_{(a)} \quad (2)$$

$$C_2H_5O_{(a)} = CH_3CHO_{(a)} + H_{(a)} \quad (3)$$

$$CH_3CHO_{(a)} = CH_3CHO_{(g)} \quad (4)$$

$$H_{(a)} + H_{(a)} = H_{2(g)} \quad (5)$$

To get some evidence about the surface stability of acetaldehyde we investigated the adsorption and reaction of CH_3CHO, too. At small gold coverages (θ_{Au} < 0.3 MLE) the adsorption of acetaldehyde was barely detectable by HREELS (not shown). As the amount of gold further increased the adsorption ability was evidently increased. At θ_{Au} ~ 1 MLE coverage the adsorbed acetaldehyde was observable; but the stability of the adsorbed molecules was very low: below room temperature almost all signs of surface fragments disappeared, only the BN phonon losses showed up. In Fig. 4.C we show the spectra of the surface layer after 170 K adsorption of acetaldehyde (saturation) on 2 MLE gold covered Rh(111); where acetaldehyde adsorption has a strong indication on the spectra. The observed vibrations at ~850, 1120, 1180, 1350, 1425 and at 2980 cm^{-1} are characteristic for acetaldehyde; nevertheless, there is a slight difference in the peak positions compared to those observed on Rh(111). In accordance with the desorption results of the mentioned analogical experiment on gold-covered BN/Rh(111) layer, only molecular acetaldehyde desorption (at ~220 K) was detected without any sign of dissociation products. On this surface layer there are no driving

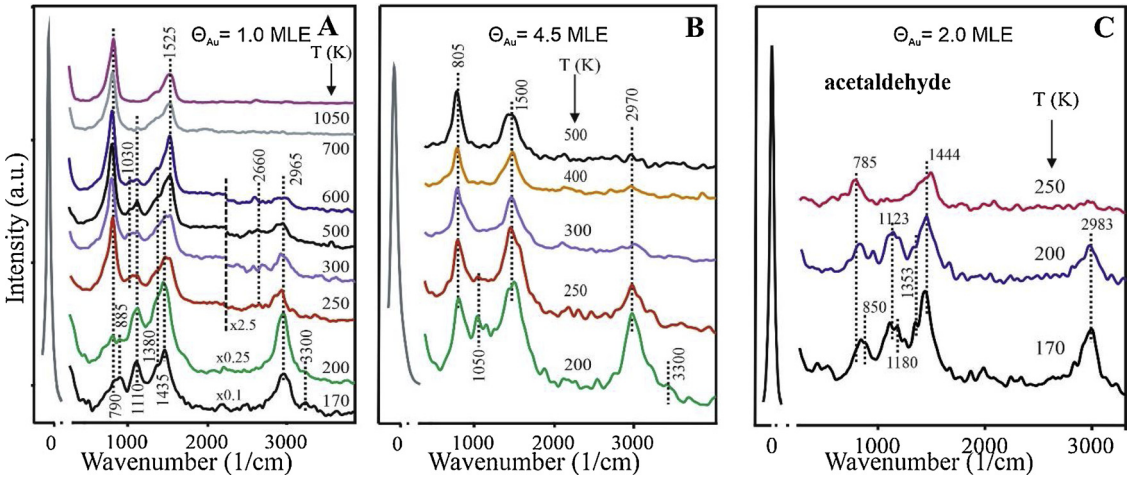

Fig. 4. Effects of annealing on the HREEL spectra after adsorption of 4 L ethanol on 1.0 MLE gold covered h-BN/Rh(111) surface at 170 K (A); on 4.5 MLE gold (B) and after adsorption of acetaldehyde on 2.0 MLE Au covered BN/Rh(111) at 170 K (C).

forces for acetaldehyde to dissociate.

The latter results confirm our concept that the reason why the ethanol dissociation process also stops at acetaldehyde is very likely the absence of suitable adsorption sites -at this temperature- on which the acetaldehyde dissociation products (e.g. CO and CH_x) can adsorb. The lack of potential adsorption sites on the BN nanomesh and the weak activity of gold toward C-C rupturing together provide a selective reaction pathway resulting in CO free hydrogen and acetaldehyde.

3.4. DFT calculation results

In this section, theoretical insights into some of the experimentally observed findings are provided by performing DFT calculations. Due to the large complexity of the above reported experimentally addressed processes, we focus on selected model systems, see Section 2 for a detailed overview. Particular focus is given on the modelling of a Au atomic cluster in the pore of h-BN/Rh(111) with differently coordinated Au atoms, and on the adsorption of ethanol and the reaction product hydrogen.

First, the energetically preferred adsorption position of a Au adatom was determined in order to find the favoured starting point for Au atomic cluster growth on the h-BN/Rh(111) surface. From the considered nine adsorption positions (see Au_1/h-BN/Rh(111) in section 2) the on-top B position in the pore region (pore-B) is clearly the preferred one with an adsorption energy of -3.21 eV, a B-Au center-to-center distance of 2.14 Å, and the Au adatom is negatively charged with 0.49 excess electron. The Au adatom started from above the pore-h position also relaxed above the pore-B position. The secondly favored Au adatom positions are close to the wall-N and wall-h surface sites with total energies of 0.46 eV above that of pore-B. Interestingly, the thirdly favored adsorption positions are pore-N and close to wall-B with total energies of 0.78 eV above that of the pore-B site. The least favored adsorption positions for the Au adatom are on the wire with total energies of at least 1.37 eV above that of pore-B.

Knowing the preferred pore-B adsorption site for the Au adatom, this has been used as the center of an initially 2D atomically flat island consisting of 19 Au atoms. This structure corresponds to a Au island with three differently coordinated Au atoms (Au-m, Au-e, Au-v) in the pore of the h-BN/Rh(111) surface, see Au_{19}/h-BN/Rh(111) in Section 2 and Fig. 5. During geometry optimization the central Au atom was shifted away from the pore-B site, and the equilibrium (pore-B)-(Au-m) distance was found 3.48 Å. Interestingly, the rest of the atoms in the Au island did not move away that much from the h-BN, and the result is a slightly bent Au island with a geometrical corrugation of 0.82 Å, where the Au-e and Au-v atoms are on average 0.48 Å and 0.81 Å lower, respectively, than the Au-m position. Bader charge analysis showed that all Au atoms of the island are negatively charged, but in different extent according to their positions: Au-m (Au-coordination: 6): -0.004 |e|; average of the six 1st shell atoms around Au-m (Au-coordination: 6): -0.005 |e|; average of the six Au-e atoms (Au-coordination: 4): -0.14 |e|; and average of the six Au-v atoms (Au-coordination: 3): -0.21 |e|. This finding explains the catalytic activity of the low-coordinated Au atoms (Au-e and Au-v) at the rim of the island.

Directly related to the experimental results in the present paper, as a next step, the energetically preferred adsorption positions of a H adatom (product of ethanol dehydrogenation) on the pure h-BN/Rh (111) and on the Au_{19} island on h-BN/Rh(111) were determined. For H/h-BN/Rh(111), just as in the Au adatom case, we find the preferred H adsorption site at the on-top B position in the pore region (pore-B) with an adsorption energy of -4.83 eV, a B-H center-to-center distance of 1.23 Å, and the H adatom is negatively charged with 0.52 excess electron. The secondly favored H adatom position is above the pore-N with a total energy of 0.94 eV above that of pore-B. H adsorption on the wall and wire of h-BN is even less favored (total energies between $1-2$ eV above that of pore-B), and the least favored adsorption position was found close to the pore-h with a total energy of 2.19 eV above that of the pore-B site.

The preference for H adsorption in the presence of a Au_{19} island on the h-BN/Rh(111) is considerably changed, partly due to the fact that much of the pore region of h-BN is covered with Au (see H/Au_{19}/h-BN/Rh(111) in section 2). In this case, the preferred H adsorption sites are always close to the Au island, and particularly close to the edge of the island, see Fig. 5. The most favored H position after geometry optimization was found where the H binds to one Au-v and one Au-e atom (Fig. 5A) at the same height level as Au-e and Au-v (The H-bound Au-v is now lifted up to the level of Au-e compared to that of the Au_{19}/BN/Rh(111) case). Here, the adsorption energy is -3.63 eV, the H adatom is negatively charged with 0.08 excess electron, and the following effective Bader charges are found for the Au atoms in the Au_{19} island: Au-m (Au-coordination: 6): +0.003 |e|; average of the six 1st shell atoms around Au-m (Au-coordination: 6): -0.009 |e|; average of the six Au-e atoms (Au-coordination: 4): -0.13 |e|; and average of the six Au-v atoms (Au-coordination: 3): -0.19 |e|. This relaxed configuration was obtained from the H atom initially sitting above a Au-v site. Two other considered H adsorption positions close to the Au island are: (i) H is solely bound to Au-e at the same height level (Fig. 5B), and (ii) H is above the Au island at a Au hollow site close to Au-m (Fig. 5C). These configurations have 0.30 eV and 0.55 eV larger total energies, respectively, compared to the energetically favoured H bound to Au-e and Au-v (Fig. 5A). H adsorption on the wall and wire of h-BN, in the presence of the Au island in the pore, is much less favoured (total energies between 1.2–2.2 eV above that of the preferred H site), and, interestingly, the least favoured H adsorption position was found on top of the B atom in the wire (wire-B site).

Finally, as the main topic of the present paper, ethanol adsorption on the pure h-BN/Rh(111) and on the Au_{19} island on h-BN/Rh(111) was studied. For both Ethanol/h-BN/Rh(111) and Ethanol/Au_{19}/h-BN/Rh(111) we considered five differently oriented ethanol molecules in

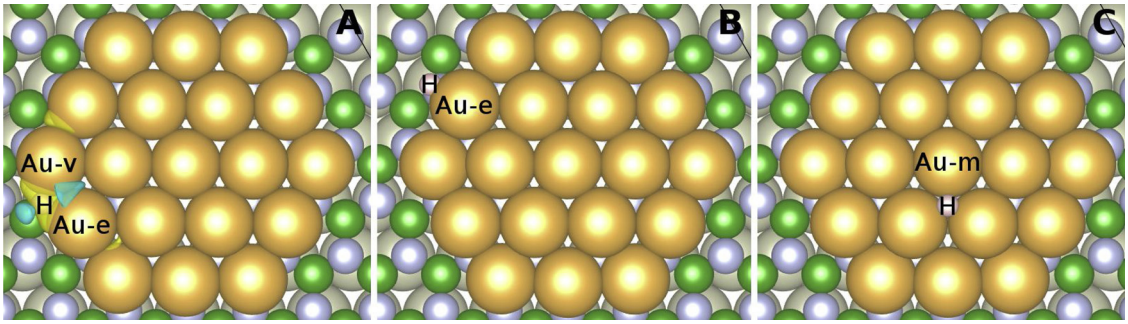

Fig. 5. Three relaxed H adsorption positions (top views) close to the Au_{19} island in the pore of h-BN/Rh(111). The charge transfer of the energetically preferred configuration upon H adsorption is explicitly shown in A (isosurface value: 0.001 |e|/Å^3; yellow: electron accumulation, blue: electron depletion). Three different Au sites of the island are indicated as Au-m, Au-e, and Au-v (For interpretation of the references to colour in this figure legend, the reader is referred to the web version of this article).

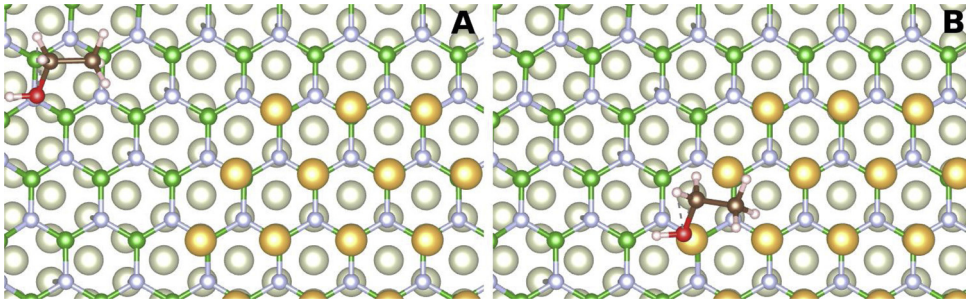

Fig. 6. The two most favored ethanol adsorption configurations above Au_{19}/h-BN/Rh(111): O above wall-N (A, energetically preferred), O close to Au-v (B, total energy higher by 11 meV than A).

Table 2
Relative total energy ranges for considered ethanol adsorption configurations on various surface regions of pure h-BN/Rh(111) and of a Au_{19} island in the pore of h-BN/Rh(111).

	Relative total energy ranges (eV)
Ethanol/BN/Rh(111)	
pore (10 configurations):	0.00-0.17
wall (10 configurations):	0.01-0.21
wire (10 configurations):	0.08-0.23
Ethanol/Au_{19}/BN/Rh(111)	
Au (15 configurations):	0.01-0.24
wall (10 configurations):	0.00-0.20
wire (10 configurations):	0.08-0.22

combination with selected characteristic surface adsorption sites (see Section 2). After geometry optimizations at T = 0 K we collected the total energies of the relaxed configurations, and the ranges of total energies in the characteristic surface areas are summarized in Table 2. As can be seen, the total energy ranges are quite narrow (0-0.24 eV) and they considerably overlap in the different surface areas, irrespectively whether a Au island is present on the h-BN/Rh(111) surface or not. Therefore, and also given the experimental temperature range, it is hard to conclude on a particularly favored adsorption geometry of ethanol on any of the studied surfaces. These findings are practically insensitive to the inclusion or lack of dipole corrections in the DFT calculation of the total energies, and they support the experimental finding of a very weak interaction between ethanol and h-BN, even if Au is present in a small quantity on h-BN (compare the HREELS results for pure h-BN/Rh(111) and Θ_{Au} = 0.2 MLE in Fig. 2A, which are very similar). It is important to mention that in the experiments the best stability of ethanol on gold was achieved above 1 ML Au coverage, which was not studied by DFT. This already suggests that if a high Au coverage is needed to increase the stability of ethanol adsorption then there is a practically uniform (and weak) adsorption character of ethanol on both h-BN and Au/h-BN below the 1 ML gold coverage. Our DFT results indeed confirm this suggestion.

Fig. 6 shows the two most favored (among the studied 35) ethanol adsorption configurations above Au_{19}/h-BN/Rh(111). A preferred parallel orientation of the C—C bond of ethanol with respect to the substrate is found similarly to transition metal substrates studied earlier with DFT + vdW method [71]. For the two configurations in Fig. 6 the calculated total energies (at T = 0 K) are very close (11 meV/supercell difference) in favor of the ethanol adsorbed on the wall region of the h-BN rather than close to the Au_{19} island, but this tiny energy difference (11 meV corresponds to T ~ 130 K) does not allow for a clear conclusion of a better wall-adsorption of ethanol when taking into account the experimental temperature range (> 130 K), or the ethanol quantity. Furthermore, we found nine other wall-adsorbed ethanol configurations, which are energetically less favored compared to the best gold-adsorbed ethanol (see the energy ranges in Table 2), and such statistics have an effect at finite temperatures. Note that the ethanol adsorption also depends very much on the molecular coverage, and, as the experimental results show, on the gold coverage, which were not studied by DFT in the present work due to the extremely large computational effort.

4. Conclusions

In this study we investigated the reactivity of the gold-covered BN/Rh(111) surface toward ethanol. We observed that the Au/h-BN/Rh(111) increased the stability of molecules and was active in the dehydrogenation process of ethanol. With coverage dependent experimental studies we determined that the active sites of gold clusters on h-BN are very likely the edge and corner atoms on the interface of gold/BN nanomesh. The presence of these sites is expected in an increased number at small coverages where pores are almost filled up with gold. We also need to count with a charge transfer between the substrate and gold which also takes place at lower coverages and resulted in negatively charged particles. As a consequence of these findings BN serves not only as an inert template for gold nanoparticles, but it can also participate in the reactions acting as a partner in dehydrogenation processes by the active contribution of boron atoms. Nevertheless, we can also state that the deficit of the possible C—C bond breaking adsorption sites on BN (and at the same time on Au as well) results in a surface layer on which a controlled dissociation of ethanol occurs. This way Au/BN serves a good product selectivity in the ethanol dissociation process producing carbon-free hydrogen and acetaldehyde. DFT calculation results provided important insights into the adsorption characteristics of ethanol and the reaction product H on model (Au)/h-BN/Rh(111) surfaces. We highlight that the extent of negative charge of Au atoms on h-BN/Rh(111) depends on their Au-coordination in Au nanostructures, and larger negative charges on low-coordinated Au atoms are responsible for their enhanced catalytic activity.

CRediT authorship contribution statement

Arnold P. Farkas: Conceptualization, Methodology, Writing - original draft, Supervision, Validation. **Ádám Szitás:** Investigation, Methodology, Visualization. **Dániel Jurdi:** Investigation. **Krisztián Palotás:** Formal analysis, Software, Writing - review & editing, Validation. **János Kiss:** Conceptualization, Writing - review & editing. **Zoltán Kónya:** Supervision, Funding acquisition.

Acknowledgments

Financial supports from the National Research Development and Innovation Office of Hungary projects No. K120115 and No. FK124100 are gratefully acknowledged. This research was also supported by the European Union and the State of Hungary, co-financed by the European Social Fund in the framework of TÁMOP-4.2.4.A/ 2-11/1-2012-0001 'National Excellence Program'. The ELI-ALPS project (GINOP-2.3.6-15-

2015-00001) is supported by the European Union and co-financed by the European Regional Development Fund.

References

[1] L. Song, L. Ci, H. Lu, P.B. Sorokin, C. Jin, J. Ni, A.G. Kvashnin, D.G. Kvashnin, J. Lou, B.I. Yakobson, P.M. Ajayan, Nano Lett. 10 (2010) 3209–3215.
[2] W. Auwärter, T.J. Kreutz, T. Greber, J. Osterwalder, Surf. Sci. 429 (1999) 229–236.
[3] W. Auwärter, M. Muntwiler, J. Osterwalder, T. Greber, Surf. Sci. 545 (2003) L735–L740.
[4] W. Auwärter, Surf. Sci. Rep. 74 (2019) 1–95.
[5] A. Nagashima, N. Tejima, Y. Gamou, T. Kawai, C. Oshima, Phys. Rev. B 51 (1995) 4606–4613.
[6] V.L. Solozhenko, A.G. Lazarenko, J.P. Petitet, A.V. Kanaev, J. Phys. Chem. Solids 62 (2001) 1331–1334.
[7] K. Watanabe, T. Taniguchi, H. Kanda, Nat. Mater. 3 (2004) 404–409.
[8] L. Britnell, R.V. Gorbachev, R. Jalil, B.D. Belle, F. Schedin, A. Mishchenko, T. Georgiou, M.I. Katsnelson, L. Eaves, S.V. Morozov, N.M.R. Peres, J. Leist, A.K. Geim, K.S. Novoselov, L.A. Ponomarenko, Science 335 (2012) 947–950.
[9] S.J. Kang, G.H. Lee, Y.J. Yu, Y. Zhao, B. Kim, K. Watanabe, T. Taniguchi, J. Hone, P. Kim, C. Nuckolls, Adv. Funct. Mater. 24 (2014) 5157–5163.
[10] D. Usachov, V.K. Adamchuk, D. Haberer, A. Grüneis, H. Sachdev, A.B. Preobrajenski, C. Laubschat, D.V. Vyalikh, Phys. Rev. B - Condens. Matter Mater. Phys. 82 (2010) 075415 1–6.
[11] Z. Liu, L. Song, S. Zhao, J. Huang, L. Ma, J. Zhang, J. Lou, P.M. Ajayan, Nano Lett. 11 (2011) 2032–2037.
[12] M. Corso, W. Auwärter, M. Muntwiler, A. Tamai, T. Greber, J. Osterwalder, Science 303 (2004) 217–220.
[13] R. Laskowski, P. Blaha, J. Phys. Condens. Matter 20 (2008) 064207 1-6.
[14] I. Brihuega, C.H. Michaelis, J. Zhang, S. Bose, V. Sessi, J. Honolka, M. Alexander Schneider, A. Enders, K. Kern, Surf. Sci. 602 (2008) L95–L99.
[15] M. Turner, V.B. Golovko, O.P.H. Vaughan, P. Abdulkin, A. Berenguer-Murcia, M.S. Tikhov, B.F.G. Johnson, R.M. Lambert, Nature 454 (2008) 981–983.
[16] M. Haruta, Catal. Today 36 (1997) 153–166.
[17] H. Huber, D. McIntosh, G.A. Ozin, Inorg. Chem. 16 (1977) 975–979.
[18] G.R. Bamwenda, S. Tsubota, T. Nakamura, M.H. Ã, Catal. Lett. 44 (1997) 83–87.
[19] S.D. Lin, M. Bollinger, M.A. Vannice, Catal. Lett. 17 (1993) 245–262.
[20] F. Boccuzzi, G. Cerrato, F. Pinna, G. Strukul, J. Phys. Chem. B 102 (1998) 5733–5736.
[21] M. Valden, X. Lai, D.W. Goodman, Science 281 (1998) 1647–1650.
[22] B. László, K. Baán, E. Varga, A. Oszkó, A. Erdőhelyi, Z. Kónya, J. Kiss, Appl. Catal. B Environ. 199 (2016) 473–484.
[23] B. László, K. Baán, A. Oszkó, A. Erdőhelyi, J. Kiss, Z. Kónya, Top. Catal. 61 (2018) 875–888.
[24] J. Kiss, Á. Kukovecz, Z. Kónya, Catal. Lett. 149 (2019) 1441–1454.
[25] H.J. Freund, N. Nilius, T. Risse, S. Schauermann, Phys. Chem. Chem. Phys. 16 (2014) 8148–8167.
[26] S. Shaikhutdinov, H.-J. Freund, Annu. Rev. Phys. Chem. 63 (2012) 619–633.
[27] T.E. James, S.L. Hemmingson, C.T. Campbell, ACS Catal. 5 (2015) 5673–5678.
[28] L. Liu, A. Corma, Chem. Rev. 118 (2018) 4981–5079.
[29] R.M. Navarro, M.A. Peña, J.L.G. Fierro, Chem. Rev. 107 (2007) 3952–3991.
[30] M. Ni, D.Y.C. Leung, M.K.H. Leung, Int. J. Hydrogen Energy 32 (2007) 3238–3247.
[31] P.D. Vaidya, A.E. Rodrigues, Chem. Eng. J. 117 (2006) 39–49.
[32] P.R.D. La Piscina, N. Homs, Chem. Soc. Rev. 37 (2008) 2459–2467.
[33] L.V. Mattos, G. Jacobs, B.H. Davis, F.B. Noronha, Chem. Rev. 112 (2012) 4094–4123.
[34] Z. Ferencz, A. Erdohelyi, K. Baán, A. Oszkó, L. Óvári, Z. Kónya, C. Papp, H.P. Steinrück, J. Kiss, ACS Catal. 4 (2014) 1205–1218.
[35] J.I. Di Cosimo, V.K. Díez, M. Xu, E. Iglesia, C.R. Apesteguía, J. Catal. 178 (1998) 499–510.
[36] I. Takahara, M. Saito, M. Inaba, K. Murata, Catal. Lett. 105 (2005) 249–252.
[37] M. Inaba, K. Murata, M. Saito, I. Takahara, React. Kinet. Catal. Lett. 88 (2006) 135–142.
[38] I.I. Soykal, H. Sohn, U.S. Ozkan, ACS Catal. 2 (2012) 2335–2348.
[39] A. Gazsi, A. Koós, T. Bánsági, F. Solymosi, Catal. Today 160 (2011) 70–78.
[40] M. Szabó, G. Halasi, A. Sápi, K.L. Juhász, J. Kiss, Á. Kukovecz, Z. Kónya, J. Nanosci. Nanotechnol. 19 (2019) 478–483.
[41] Y. Guan, E.J.M. Hensen, Appl. Catal. A Gen. 361 (2009) 49–56.
[42] P.Y. Sheng, G.A. Bowmaker, H. Idriss, Appl. Catal. A Gen. 261 (2004) 171–181.
[43] C.A. Carrero, W.P. McDermott, S.E. Specht, J.T. Grant, A. Chieregato, F. Goeltl, S.P. Burt, J. Venegas, I. Hermans, P. Mueller, Science 354 (2016) 1570–1573.
[44] L. Shi, D. Wang, W. Song, D. Shao, W.P. Zhang, A.H. Lu, ChemCatChem 9 (2017) 1788–1793.
[45] L. Liu, Z. Zhou, Q. Guo, Z. Yan, Y. Yao, D.W. Goodman, Surf. Sci. 605 (2011) L47–L50.
[46] Y. Zhang, Y. Zhang, D. Ma, Q. Ji, W. Fang, J. Shi, T. Gao, M. Liu, Y. Gao, Y. Chen, L. Xu, Z. Liu, Nano Res. 6 (2013) 887–896.
[47] K. Gotterbarm, F. Späth, U. Bauer, C. Bronnbauer, H.P. Steinrück, C. Papp, ACS Catal. 5 (2015) 2397–2403.
[48] M.L. Ng, A.B. Preobrajenski, A.S. Vinogradov, N. Mårtensson, Surf. Sci. 602 (2008) 1250–1255.
[49] H.P. Koch, R. Laskowski, P. Blaha, K. Schwarz, Phys. Rev. B - Condens. Matter Mater. Phys. 86 (2012) 1–7.
[50] M.C. Patterson, B.F. Habenicht, R.L. Kurtz, L. Liu, Y. Xu, P.T. Sprunger, Phys. Rev. B – Condens. Matter Mater. Phys. 89 (2014) 1–10.
[51] R. Gubó, G. Vári, J. Kiss, A.P. Farkas, K. Palotás, L. Óvári, A. Berkó, Z. Kónya, Phys. Chem. Chem. Phys. 20 (2018) 15473–15485.
[52] A.P. Farkas, Á. Szitás, G. Vári, R. Gubó, L. Óvári, A. Berkó, J. Kiss, Z. Kónya, Top. Catal. 61 (2018) 1247–1256.
[53] L. Óvári, A. Berkó, G. Vári, R. Gubó, A.P. Farkas, Z. Kónya, Phys. Chem. Chem. Phys. 18 (2016) 25230–25240.
[54] G. Kresse, J. Furthmüller, Phys. Rev. B - Condens. Matter Mater. Phys. 54 (1996) 11169–11186.
[55] G. Kresse, J. Furthmüller, Comput. Mater. Sci. 6 (1996) 15–50.
[56] G. Kresse, D. Joubert, Phys. Rev. B - Condens. Matter Mater. Phys. 59 (1999) 1758–1775.
[57] J. Klimeš, D.R. Bowler, A. Michaelides, J. Phys. Condens. Matter 22 (2010) 022201 1-5.
[58] J. Klimeš, D.R. Bowler, A. Michaelides, Phys. Rev. B – Condens. Matter Mater. Phys. 83 (2011) 195131 1–13.
[59] W. Tang, E. Sanville, G. Henkelman, J. Phys. Condens. Matter 21 (2009) 084204 1–7.
[60] E. Sanville, S.D. Kenny, R. Smith, G. Henkelman, J. Comput. Chem. 28 (2007) 899–908.
[61] G. Henkelman, A. Arnaldsson, H. Jónsson, Comput. Mater. Sci. 36 (2006) 354–360.
[62] X. Xu, C.M. Friend, Surf. Sci. 260 (1992) 14–22.
[63] D.C. Papageorgopoulos, Q. Ge, D.A. King, J. Phys. Chem. 99 (1995) 17645–17649.
[64] C.J. Houtman, M.A. Barteau, J. Catal. 130 (1991) 528–546.
[65] I. Kovács, A.P. Farkas, Á. Szitás, Z. Kónya, J. Kiss, Surf. Sci. 664 (2017) 129–136.
[66] A.F. Lee, D.E. Gawthrope, N.J. Hart, K. Wilson, Surf. Sci. 548 (2004) 200–208.
[67] S. Linic, M.A. Barteau, J. Am. Chem. Soc. 124 (2002) 310–317.
[68] A.P. Farkas, P. Török, F. Solymosi, J. Kiss, Z. Kónya, Appl. Surf. Sci. 354 (2015) 367–372.
[69] G.S. Jones, M. Mavrikakis, M.A. Barteau, J.M. Vohs, J. Am. Chem. Soc. 120 (1998) 3196–3204.
[70] W.C. McKee, M.C. Patterson, D. Huang, J.R. Frick, R.L. Kurtz, P.T. Sprunger, L. Liu, Y. Xu, J. Phys. Chem. C 120 (2016) 10909–10918.
[71] R.L.H. Freire, A. Kiejna, J.L.F. Da Silva, Phys. Chem. Chem. Phys. 18 (2016) 29526–29536.